Integrated Modified Rectangular Loop Slot Antenna on Substrate Lenses for Millimeter- and Submillimeter-Wave Frequencies Mixer Applications

Pablo Otero, George V. Eleftheriades, *Member, IEEE*, and Juan R. Mosig, *Senior Member, IEEE*

Abstract— In this work, a coplanar waveguide (CPW)-fed rectangular-loop slot antenna with built-in tuning and dc-return capabilities on extended hemispherical lenses is examined. The proposed configuration is scalable up to the submillimeter-wave frequencies. For designing and analyzing the impedance characteristics of the proposed antenna, a multilayer method of moments (MoM) solver has been developed based on the mixed potential integral equation (MPIE) formulation. The corresponding patterns through the lens are obtained using geometrical optics and the surface equivalence principle. Three models have been simulated and one of them has been built and tested at 65 GHz. The integrated antenna exhibits tuning capability, rotationally symmetric patterns, high directivity, good Gaussian coupling efficiency, and a reasonable bandwidth. In addition, computed results agree well with measurements and are used to characterize the input impedance and pattern behavior of the antenna.

Index Terms—Slot antennas.

I. INTRODUCTION

IN RECENT years, there has been an increasing interest in replacing traditional waveguide-based Schottky diode mixers with printed integrated-circuit ones in the millimeter- and submillimeter-wave bands. However, at these high frequencies, the excitation of surface waves in printed dielectric substrates introduces a serious limitation. A successful approach to eliminate surface-wave losses is to print the antenna/mixer configuration on the back surface of extended dielectric-substrate lenses [1]. In this assembly, a planar antenna feed is located at the center of the back surface. Both printed strip- and slot-type antennas have been tried for antenna feeds. Slot antennas seem to be preferred in the literature because the ground plane in which they are etched isolates the front and the back half-spaces, leading to better radiation diagrams. When a rotationally symmetric main beam is needed, a very good choice is the twin-slot antenna. A monolithically integrated twin-slot Schottky diode mixer was tested successfully at

250 GHz in uniplanar coplanar waveguide (CPW) (also known as coplanar transmission line) technology, by Gearhart and Rebeiz [2]. In addition to rotationally symmetric patterns, the twin-slot configuration provides a wide bandwidth and simple matching and dc return for Schottky mixing devices. Unfortunately, the twin-slot planar mixer approach becomes difficult to realize at submillimeter-wave frequencies. This limitation stems from the short distance between the slots, required to achieve rotationally symmetric patterns. To overcome this difficulty, the twin slots can be replaced by loop-slot-type antennas [3]–[5]. This allows to separate the antenna from the mixing device and, thus, should enable the realization of integrated antenna mixers at submillimeter-wave frequencies. CPW technology provides a very convenient feed structure to excite balanced slot antennas etched in a ground plane. Moreover, the CPW line is an uniplanar technology allowing for the easy integration of active devices, leading to a simple manufacturing processes. As a consequence, an increasing interest in the CPW feed mechanism is observed in recent literature [4], [6], [7].

In this work, a new type of CPW-fed rectangular-loop-slot antenna is introduced as an alternative to the twin-slot solution for feeding dielectric substrate lenses. The new feed-element features built-in dc-return and tuning capabilities, while still providing symmetric patterns like the twin-slot configuration; however, unlike the twin-slot feed, the new rectangular-loop slot element can be easily scaled to submillimeter-wave frequencies. In addition, the new design offers flexibility in adjusting the antenna pattern symmetry and input impedance by tuning the loop-aspect ratio. Moreover, the built-in integrated stub tuner (IST) not only helps tuning the antenna, but also balances the geometry, thus helping to maintain the overall pattern symmetry. For the design and analysis of the new structures, a general full-wave analysis technique based on the mixed-potential integral equation formulation and the method of moments (MoM) has been developed. The technique utilizes subdomain rooftop-basis functions and a customized modular mesh generator [9] allowing great flexibility in modeling general arbitrary geometries printed on substrate lenses. Furthermore, the technique is capable of handling multilayer substrates attached at the back surface of substrate lenses. Patterns through the lens are computed using Fresnel coefficients and the surface equivalence principle [10]. Section II provides a short description of the analytical method.

P. Otero and J. R. Mosig are with the Electromagnetics and Acoustics Laboratory (LEMA), Swiss Federal Institute of Technology, Lausanne (EPFL), Switzerland.

G. V. Eleftheriades was formerly with LEMA-EPFL. He is now with the University of Toronto, Toronto, ON M5S 3G4 Canada.

The full description of the new antenna is given in Section III. Three 10 : 1 scaled models of the desired 650-GHz band antenna (the intended application being satellite-based remote sensing of the atmosphere) have been used for simulating and testing purposes. The first one, with a nominal frequency of 60 GHz, has been analyzed to determine input admittance, return loss, and tuning performance versus IST length and slot width. The second model is used for investigating the lens antenna bandwidth versus loop-aspect ratio. The third model, intended to operate between 65–70 GHz, has been simulated, built, and measured. It is worth noting that the return loss is computed with reference to a matching load of $50-j50~\Omega$, which is a typical input impedance for Schottky diodes. Simulations results have been verified by measurements. Simulated and measured results are described in Section IV.

II. ANALYTICAL METHOD

A. The Mixed-Potential Integral Equation (MPIE)

Our integrated antenna mixer is shown in Fig. 1. The ground plane is a conductor layer on the back surface of a dielectric lens. If the lens radius is much larger than the wavelength in the dielectric, the slots may be considered to be etched in a conductor plane between two homogeneous half-spaces. One possible equation governing this structure is the magnetic formulation of the MPIE, which is obtained when the integral representations of the magnetic field above and below the slot's plane are forced to satisfy the boundary condition of the magnetic field $\overline{H}$. Let $z = 0$ be the plane where the slot is etched in Fig. 1. Proceeding as explained, the MPIE can be written as [11]

$$
\frac{j}{\omega}\nabla_t \iint_{\text{slot}} G_W(x,y|x',y')\nabla' \cdot \overline{M}_s \, dS'
$$
$$
+ j\omega \iint_{\text{slot}} \overline{\overline{G}}_F(x,y|x',y') \cdot \overline{M}_s \, dS'
$$
$$
= \hat{z} \times \overline{J}^{exc}{}_s \quad \text{A/m} \tag{1}
$$

where $\overline{M}_s$ is the equivalent magnetic current source of the electromagnetic field, $\overline{\overline{G}}_F$ is the Green's dyadic of the electric vector potential $\overline{F}$, G_W is the Green's function of the magnetic scalar potential W, and $\overline{J}^{exc}_s$ is an exciting electric current linear density that vanishes everywhere on the plane $z = 0$ except at the location where the slot is fed [12]. Because of the reciprocity theorem, the antenna part of the circuit, shown in Fig. 1 at the right-hand side of the plane $A–A'$, may be analyzed as if it was a transmitting antenna. In this case, $\overline{J}^{exc}_s$ is introduced by an external guiding structure such as a coaxial cable, which, in turn, feeds the CPW section at the plane $A–A'$ [13]. The input impedance and the return loss of the receiving antenna will be the same as those of the transmitting antenna.

B. Green's Functions

The kernels of the two integrals appearing in the MPIE (1) are the sum of the Green's functions above and below the
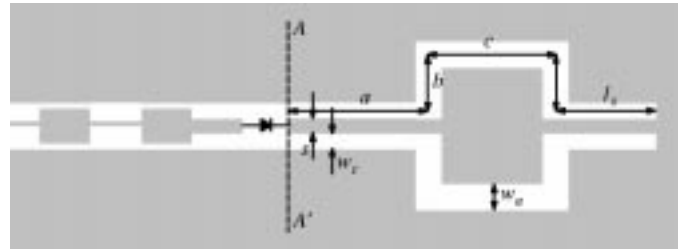

Fig. 1. Integrated mixer and rectangular slot loop with IST.

ground plane, calculated at $z = z' = 0$; that is,

$$
G_W(x,y|x',y') = G_{Wu}(x,y,0|x',y',0)
$$
$$
+ G_{Wl}(x,y,0|x',y',0) \tag{2}
$$
$$
\overline{\overline{G}}_F(x,y|x',y') = \overline{\overline{G}}_{Fu}(x,y,0|x',y',0)
$$
$$
+ \overline{\overline{G}}_{Fl}(x,y,0|x',y',0). \tag{3}
$$

The ground plane in which the slots are etched divides the space into two semi-infinite half-spaces. The electromagnetic problem in both half-spaces are independent. Moreover, the two half-spaces are similar and the process of calculating the Green's functions is identical at both sides of the plane. This process is extremely simplified when done in the spectral domain. Because of the rotational symmetry of the concerned structure, the transformation into the spectral domain is accomplished by means of the Sommerfeld's integral [14].

Mosig [15] has calculated the spectral domain Green's functions for electric sources in a planar multilayer structure. Proceeding in a similar way for magnetic currents leads to the following. Any component $\tilde{\Psi}$ of the spectral domain Green's functions in the nth layer of the structure may be written as

$$
\tilde{\Psi} = a_n \cosh(zu_n) + b_n \sinh(zu_n) \tag{4}
$$

where u contains the spectral variable k_ρ

$$
u_n^2 = k_\rho^2 - k_n^2 = k_\rho^2 - \omega^2 \mu_n \varepsilon_n. \tag{5}
$$

The coefficients a_n and b_n are shown in Table I. The variables t_{ij} in Table I are the four elements of the *total transmission matrix* T, which is the product of the n-transmission matrices defined at every interface between the $n+1$ layers composing the structure [15]

$$
T = \begin{pmatrix} t_{11} & t_{12} \\ t_{21} & t_{22} \end{pmatrix}
$$
$$
= \prod_{i=1}^{n} T_{i-1,i}
$$
$$
= \prod_{i=1}^{n} \begin{pmatrix} \alpha_i c_i/\alpha_{i-1} & \alpha_i s_i/\alpha_{i-1} \\ u_i s_i/u_{i-1} & u_i c_i/u_{i-1} \end{pmatrix} \tag{6}
$$

with

$$
\alpha_i = \begin{cases} \epsilon_i, & \text{if } \tilde{\Psi} \text{ represents an electric component;} \\ \mu_i, & \text{if } \tilde{\Psi} \text{ represents a magnetic component;} \end{cases}
$$
$$
c_i = \cosh(h_i u_i);
$$
$$
s_i = \sinh(h_i u_i);
$$
$$
h_i \quad \text{thickness of layer } i.
$$

TABLE I
COEFFICIENTS OF THE SPECTRAL GREEN'S DYADICS COMPONENTS

	$\tilde{G}_E^{zx}$	$\tilde{G}_E^{zy}$	$\tilde{G}_E^{zz}$
b_n	$k_y/j2\pi u_n$	$-k_x/j2\pi u_n$	0
a_n	$-b_n(t_{12}+t_{22})/(t_{11}+t_{21})$		
	$\tilde{G}_H^{zx}$	$\tilde{G}_H^{zy}$	$\tilde{G}_H^{zz}$
a_n	$-k_x/2\pi\omega\mu_n$	$-k_y/2\pi\omega\mu_n$	0
b_n	$-a_n(t_{11}+t_{21})/(t_{12}+t_{22})$		

Once the spectral Green's functions of the fields are known, the spectral Green's functions of the Sommerfeld's choice potentials can be calculated as follows, where only the components needed for the concerned problem are shown [15]:

$$\tilde{G}_F^{xx} = \tilde{G}_F^{yy} = j\frac{\epsilon_n}{k_y}\tilde{G}_E^{zx} \tag{7}$$

$$\tilde{G}_W = \frac{j}{\mu_n k_y}(k_n/k_r)^2\tilde{G}_E^{zx} - \frac{\omega}{k_x k_r^2}\frac{\partial\tilde{G}_H^{zx}}{\partial z}. \tag{8}$$

Once the spectral Green's functions for the potentials are known, the spatial Green's functions can be calculated by means of the Sommerfeld's integral.

To build the scaled prototypes, a machined ceramic lens is used and the antenna is etched in a Duroid substrate of a different permittivity (10.8 instead of 11.7 of the final Silicon lens). Therefore, a tool capable of analyzing the planar stratified half-space is needed.

C. Method of Moments

To solve the MPIE (1), a computer program which implements the MoM has been developed. The unknown $\overline{M}_s$ is approximated by a linear combination of *basis* functions B_{xi} and B_{yi}, weighted by complex scalar coefficients c_{xk} and c_{yk}

$$\overline{M}_s = \sum_{k=1}^{N_x}\hat{x}c_{xk}B_{xk} + \sum_{k=1}^{N_y}\hat{y}c_{yk}B_{yk}. \tag{9}$$

The basis functions chosen are usually referred to as "subdomain rooftops." They are defined only in small rectangles $(x_{Bli} \le x \le x_{Bri}, y_{Blj} \le y \le y_{Brj})$ in the following way:

$$B_{xk} = T_i(x)P_j(y) \tag{10}$$

and the rooftop along the y axis is

$$B_{yk} = P_i(x)T_j(y) \tag{11}$$

that is, the product of a subsectional *triangle function* T_i along one of the axes times a subsectional *pulse function* P_j along the normal axis

$$T_i(x) = \begin{cases} (x-x_{Bi\ell})/(x_{Bio}-x_{Bi\ell}) & x_{Bi\ell} \le x \le x_{Bio} \\ (x-x_{Bir})/(x_{Bio}-x_{Bir}) & x_{Bio} \le x \le x_{Bir} \\ 0 & \text{elsewhere} \end{cases} \tag{12}$$

$$P_j(y) = \begin{cases} 1 & y_{Bi\ell} \le y \le y_{Bir} \\ 0 & \text{elsewhere} \end{cases} \tag{13}$$

and similar expressions for the rooftop function along the y axis. When substituting the expansion (9) into the MPIE (1), we arrive to an integral equation with $N_x + N_y$ unknowns, which are the scalar coefficients c_{xk} and c_{yk}

$$\frac{j}{\omega}\nabla_t \iint_{\text{slot}} G_W \nabla'\left(\sum_{k=1}^{N_x}\hat{x}c_{xk}B_{xk} + \sum_{k=1}^{N_y}\hat{y}c_{yk}B_{yk}\right)dS'$$
$$+ j\omega\iint_{\text{slot}}\overline{\overline{G}}_F\left(\sum_{k=1}^{N_x}\hat{x}c_{xk}B_{xk} + \sum_{k=1}^{N_y}\hat{y}c_{yk}B_{yk}\right)dS'$$
$$= \hat{z} \times \overline{J}_s^{exc}\text{A/m}. \tag{14}$$

We use the standard Galerkin's approach of the MoM, computing the inner product of the MPIE (14) with N_x *weighting* (or *testing*) functions $\overline{B}_{xl} = \hat{x}B_{xl}$ and N_y weighting functions $\overline{B}_{yl} = \hat{y}B_{yl}$. Written in matrix form, the set of equations that is obtained is

$$\left(j\omega\begin{pmatrix}(F_{kl}^{xx}) & (0) \\ (0) & (F_{kl}^{yy})\end{pmatrix} + \frac{j}{\omega}\begin{pmatrix}(W_{kl}^{xx}) & (W_{kl}^{xy}) \\ (W_{kl}^{yx}) & (W_{kl}^{yy})\end{pmatrix}\right)\begin{pmatrix}(c_l^x) \\ (c_l^y)\end{pmatrix}$$
$$= \begin{pmatrix}(J_k^x) \\ (J_k^y)\end{pmatrix} \tag{15}$$

or, for short writing

$$MC = J \tag{16}$$

where C is the unknown coefficients vector, M is the *moment matrix*, and J is the *excitation current vector*. Obviously, the moment matrix is square as long as the same number of basis and weighting functions are used. In addition, the matrix M is symmetric because it has been generated with a Galerkin's approach. The elements of M are

$$F_{k\ell}^{xx} = \iint_{\text{slot}}\iint_{\text{slot}} B_k^x(x,y)G_F^{xx}B_\ell^x(x',y')\,dS\,dS'$$
$$k = 1,\cdots,N_x, \quad \ell = 1,\cdots,N_x \tag{17}$$

$$W_{k\ell}^{xx} = \iint_{\text{slot}}\frac{\partial B_\ell^x}{\partial x'}\iint_{\text{slot}} G_W\frac{\partial B_k^x}{\partial x}\,dS\,dS'$$
$$k = 1,\cdots,N_x, \quad \ell = 1,\cdots,N_x \tag{18}$$

$$W_{k\ell}^{xy} = \iint_{\text{slot}}\frac{\partial B_\ell^y}{\partial y'}\iint_{\text{slot}} G_W\frac{\partial B_k^x}{\partial x}\,dS\,dS'$$
$$k = 1,\cdots,N_x, \quad \ell = 1,\cdots,N_y \tag{19}$$

and three similar equations for $F_{k\ell}^{yy}$, $W_{k\ell}^{yx}$, and $W_{k\ell}^{yy}$. The elements of J are

$$J_k^x = -\iint_{\text{slot}} B_k^x(x,y)J_{sy}^{exc}dS, \qquad k = 1,\cdots,N_x \tag{20}$$

$$J_k^y = \iint_{\text{slot}} B_k^y(x,y)J_{sx}^{exc}dS, \qquad k = 1,\cdots,N_y. \tag{21}$$

Detailed descriptions of how to numerically compute the four-fold integrals (17)–(19) containing singular Green's functions to fill the moment matrix M and how to fill the excitation current vector J can be found, respectively, in [11] and [13].

D. Input Impedance and Return Loss

Once the MoM unknown C is determined, the antenna input impedance Z_a at the plane A–A' of Fig. 1, defined for the *quasi*-TEM mode propagating in the CPW, can be calculated. This computation is closely related to the manner in which the elements of the excitation current vector J have been calculated and is described in detail in [13]. Furthermore, in [13] the method to compute the input impedance of a CPW-fed slot circuit has been validated by measurements of scaled circuits. The antenna delivers the received signal to the mixing device. The proper figure of merit of the matching between the antenna and the Schottky diode is the return loss; that is, the ratio between the available power and the reflected power. It is worth noting that Schottky diodes do not present pure real input impedances, but typically 50-$j50$ Ω at frequencies in the band of interest. When neither source nor load impedances are real, it can be easily demonstrated that the return loss is the inverse of the squared module of the conjugate reflection coefficient. Let Z_d be the typical input impedance of a Schottky diode. The return loss RL (expressed in decibels) and the conjugate reflection coefficient Γ are

$$RL = -20, \quad \log|\Gamma| = -20, \quad \log\left|\frac{Z_d - Z_a^*}{Z_d + Z_a}\right|. \quad (22)$$

E. Radiation Patterns

In the case of two homogeneous half-spaces, once the MoM unknown C vector is determined, the computation of the far fields is straightforward. In the case where the lens side of the slot is layered, a complication arises because the vector potential obtained as

$$\overline{F} = \iint_{\text{slot}} \overline{\overline{G}}_F \cdot \overline{M}_s \, dS' \quad (23)$$

needs the value of the Green's function $\overline{\overline{G}}_F(\overline{R}|\overline{R}')$ at points $k|\overline{R}| \gg 1$, which, in turn, needs the use of asymptotic techniques to compute the Sommerfeld integral [16].

The patterns of the lens antenna are computed in the following manner. The far fields of the antenna feed are computed at the inner lens surface. Fresnel coefficients are applied to compute the fields at the outer lens surface. Subsequent application of the surface equivalence principle leads to the establishment of equivalent electric and magnetic currents over the surface of the lens from which the far fields can be computed. Interested readers can refer to the work by Filipovic *et al.* [10], [17].

The analysis of propagation when working with quasi-optical instruments in these bands is mainly done by means of the theory of *Gaussian beam* propagation [18], which assumes the validity of the *paraxial* wave equation. A relevant figure of merit is the *Gaussian coupling efficiency* η_g defined as the fractional power radiated into a fundamental Gaussian mode, including polarization loss [19], [20]. To arrive to a mathematical definition for the Gaussian coupling efficiency, we use the coupling factor η_c derived by Schwarz [21] from the Lorentz reciprocity theorem. For our case, the best form

is that presented in the following [20]:

$$\eta_c = \frac{1}{4} \frac{\left|\iint_S (\overline{E}_{\text{tr}} \times \overline{H}_{inc} - \overline{E}_{inc} \times \overline{H}_{\text{tr}}) \cdot \overline{dS'}\right|^2}{\iint_S (\overline{E}_{inc} \times \overline{H}_{inc}^*) \cdot \overline{dS'} \iint_S (\overline{E}_{\text{tr}} \times \overline{H}_{\text{tr}}^*) \cdot \overline{dS'}} \quad (24)$$

where integrals are extended over a surface S that encloses the antenna. The coupling factor in (24) is not restricted to any kind of incident field. If the fields of a plane wave are used for $\overline{E}_{inc}$ and $\overline{H}_{inc}$, the traditional aperture efficiency factor is obtained. However, it should be mentioned that (24) includes not only the effect of the field distribution over the surface S but also the polarization effect. When a Gaussian mode is used in (24) for $\overline{E}_{inc}$ and $\overline{H}_{inc}$, the Gaussian coupling efficiency η_g is obtained. In addition, for the lens case, $\overline{E}_{tr}$ and $\overline{H}_{tr}$ are the far fields computed in the previous section in which case the simplest way is to take S in (24) to represent a sphere.

F. Test Set

The frequency range of our instrumentation does not enable direct input impedance or return loss measurements at 65 GHz. A pattern measurement setup based on subharmonic mixing in the millimeter-wave band (60–90 GHz) consisting basically of an optical rail, a Gunn oscillator connected to a transmitting horn antenna, a spectrum analyzer, a step-motor, and a control computer is used to measure the radiation patterns. The subharmonic mixing process is monitored automatically by the spectrum analyzer (HP-8563-E) under computer control. The intermediate frequency (IF) signal detected by the spectrum analyzer comes from mixing the received signal with the sixteenth harmonic of the local oscillator (LO) through the use of a diplexer.

III. INTEGRATED ANTENNA MIXER DESCRIPTION

In order to first validate our analytical method and second the proposed antenna feed topology, three models have been used. The dimensions shown in Fig. 1 of these three models are listed in Table II. All distances are in μm. Model A has been used to analyze the antenna-feed behavior depending on the slot width w_a and the IST length l_s. Model B has been used to analyze the behavior depending on the *aspect ratio* AR defined as

$$AR = \frac{2b}{c}. \quad (25)$$

Model C has been simulated, built, and measured. Model C incorporates the Schottky diode and an IF filter. The filter is a nine section CPW low-pass filter with a cutoff frequency of 40 GHz. The filter is depicted in Fig. 1 at the left-hand side of the diode; dimensions are omitted. In the same figure, the diode is only sketched, for the sake of clarity. The devices that have been used are Hewlett Packard GaAs detector diodes HSC-9161. Regardless of their name, they have been used as coherent mixers—not as detectors.

The final lens dielectric is supposed to be silicon of a relative permittivity of $\varepsilon_r = 11.7$. For the prototype antenna, however, the synthetic ceramic HiK, with relative permittivity

TABLE II
FEED ANTENNAS DIMENSIONS (IN MICROMETERS)

Model	w_c	s	w_a	a	b	c	l_s
A	50	50	50 100	950	290	580	318–592
B	110	180	110	905	270 334	500 620	455
C	50	50	100	850	247	574	450
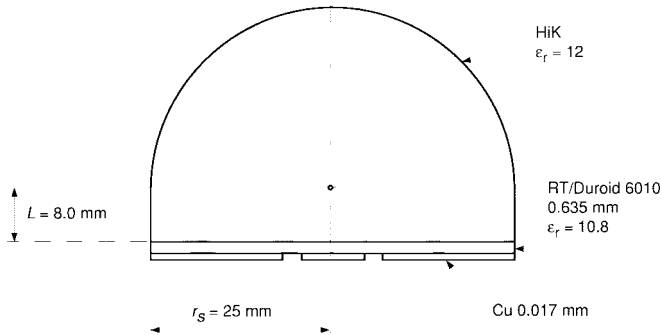
Fig. 2. Lens antenna assembly.

Fig. 3. Model A: computed input conductance versus frequency.

Fig. 4. Model A: computed input susceptance versus frequency.

of $\varepsilon_r = 12$, has been used. Also for the prototype, the antenna has not been etched in the lens but in a RT/Duroid 6010 substrate 0.635-mm-thick and of relative permittivity $\varepsilon_r = 10.8$. The lens radius is $r_s = 25$ mm; that is, about 19 times the wavelength in the dielectric for a frequency of 65 GHz. The extension lengths corresponding to hyperhemispherical and diffraction limited lenses are, respectively, $L_h = 7.2$ mm and $L_e \simeq 9.7$ mm. The extension length used is $L = 8.6$ mm, which lies between L_h an L_e. The assembly is sketched in Fig. 2.

IV. SIMULATIONS AND MEASUREMENTS

As already mentioned, the design input impedance of the proposed antenna is $50+j50$ Ω to match a typical Schottky diode; that is, an input admittance of $0.01-j0.01$ Siemens.

Figs. 3 and 4 show the conductance and susceptance, respectively, of model A *versus* frequency using the IST length as parameter l_s. Obviously, the loop size is determined by the desired frequency. However, since we do not look for a real input admittance, the loop will not operate at a resonance. Instead, for the required admittance, the region between the second and the third resonance is used, where still the patterns show a main beam broadside. Fig. 5 shows the return loss of model A *versus* frequency using the IST length l_s as parameter. With regard to tuning capability, a 5.5-GHz (9.2%) tuning range is obtained when the IST length varies between $0.7\lambda_g/4 \le l_s \le 1.3\lambda_g/4$, where λ_g is the wavelength in the CPW. The simulated half-space feed patterns of model A *versus* IST length are shown in Fig. 6. As shown, the H-plane pattern is not sensitive to l_s. From Figs. 5 and 6 we observe that longer IST stubs result in more symmetric E-plane patterns, but the price to pay is narrower bandwidth. On the other hand, shorter IST stubs result in wider bands but
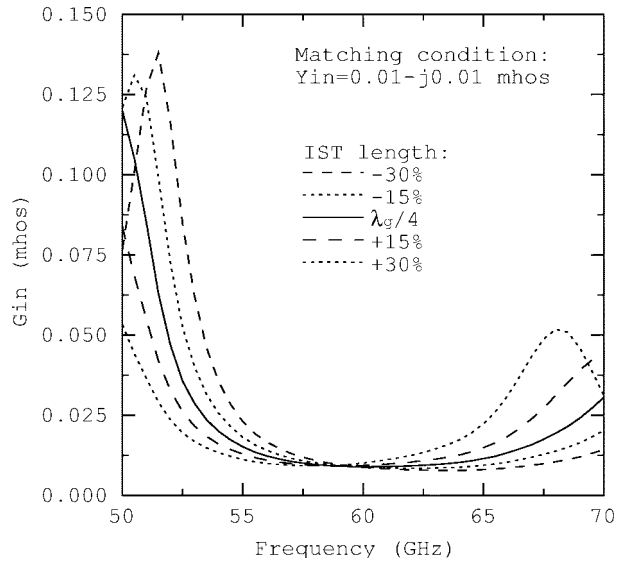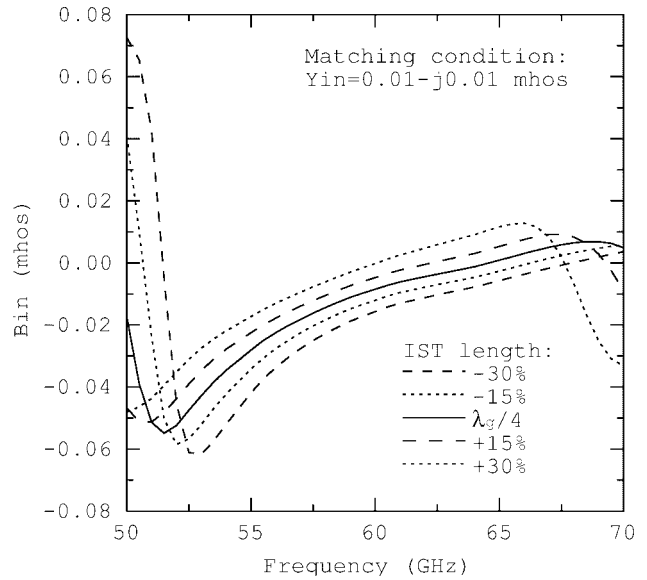
patterns deteriorate. Plotting the return loss *versus* frequency and slot width w_a, it has been found that a wider slot exhibits a wider band; a slight shift in the band frequency results as well when increasing w_a. The slot width shows a negligible effect on patterns and, hence, a wider slot should be preferred.

Model B has been used to determine the sensitivity of the return loss to the aspect ratio AR. Fig. 7 shows that the larger the AR, the better the matching is and the wider the band. This trend is opposite of the dependence on IST length and slot width, where an improvement in matching means a reduction in bandwidth and vice versa. Fig. 7 shows clearly that an eventual bandwidth requirement should be satisfied by a proper choice of aspect ratio. However, it has been found that when AR increases the patterns symmetry deteriorates. A good compromise seems to be $AR = 1$. From this value, if a slight asymmetry of the main lobe may be accepted, the frequency bandwidth increases rapidly.
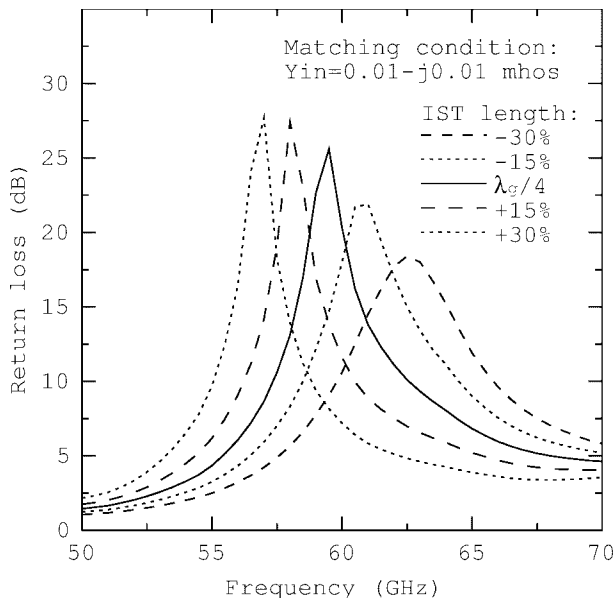
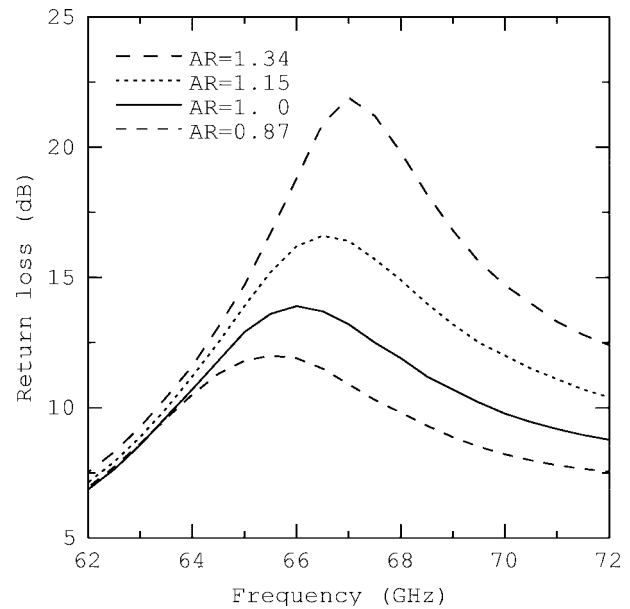Fig. 5.   Model A: computed return loss versus frequency and IST length.

Fig. 7.   Model B: computed return loss versus frequency and aspect ratio.
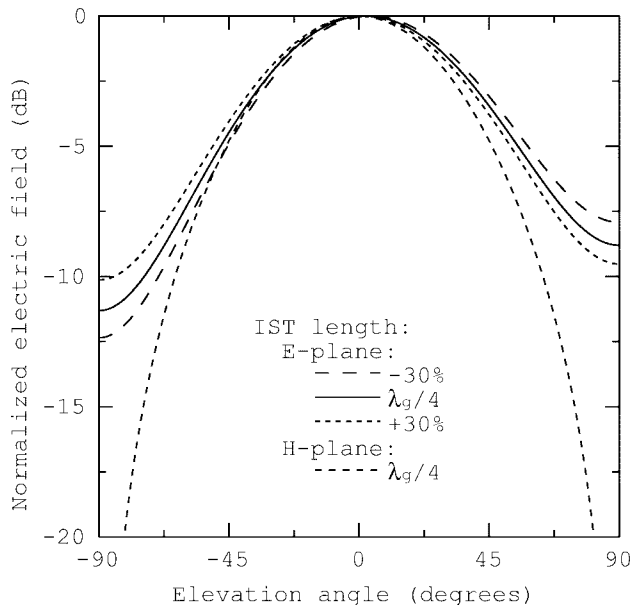

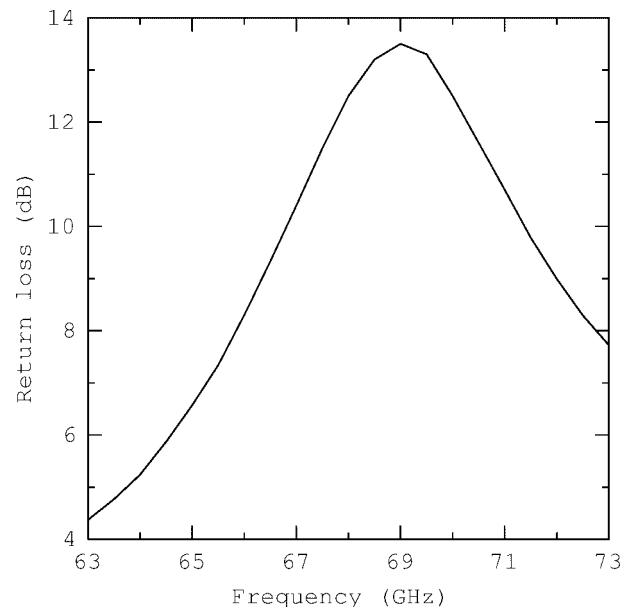Fig. 6.   Model A: computed copolar patterns inside the lens at 60 GHz.

Fig. 8.   Model C: computed return loss.

It is worth noting, however, that the lens has a smoothing effect which eventually reduces the observed antenna feed-pattern asymmetry.

Model C has been simulated, built as explained in the previous section, and measured. Computed and measured parameters of model C are shown in Figs. 8–13. Figs. 8 and 9, that show the computed return loss and copolar patterns inside the lens, respectively, are consistent with previous simulations. Fig. 10 shows the cross-polar patterns inside the lens. The lens antenna patterns, computed and measured, are shown in Figs. 11–13. In the main-lobe region, computed and measured results are in good agreement. The observed high secondary lobes in the E-plane patterns are not due to the antenna feed. Experiments have been conducted that confirm that the first sidelobe is due to the spurious radiation of the gap where the

Schottky diode is mounted. It may be observed in Figs. 11 and 13, that a difference exists between the sidelobe levels of the E-plane patterns at 70 and 72 GHz. Since theory predicts the same sidelobe level at 70 and 72 GHz, a plausible explanation for the measured difference may be attributed to the matching between the diode and the antenna. The better the matching, the larger the power received through the antenna relative to the power received through the diode gap and the lower the relative sidelobe level. The second sidelobe is due to the spurious radiation of the IF filter, and the same previous argument applies.

Computed directivity D and Gaussian coupling efficiency η_g when using the HiK lens with an extension length of 9.1 mm at 70 GHz, are, respectively, 31 dB and 86%. The computed transmission efficiency due to reflection on the lens
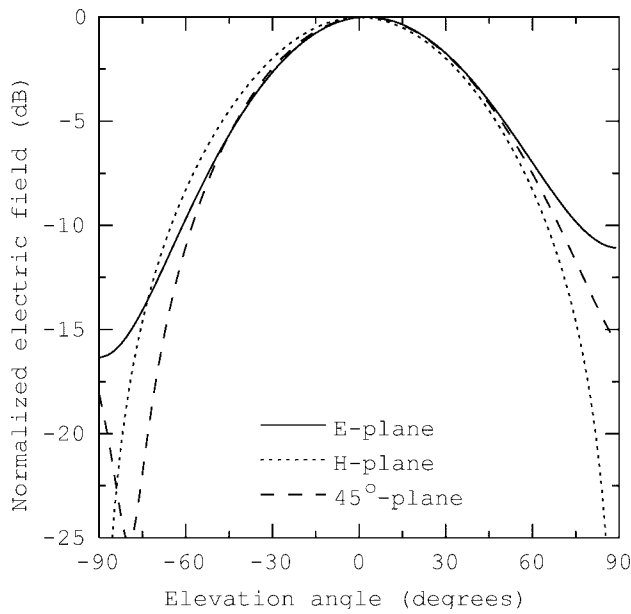
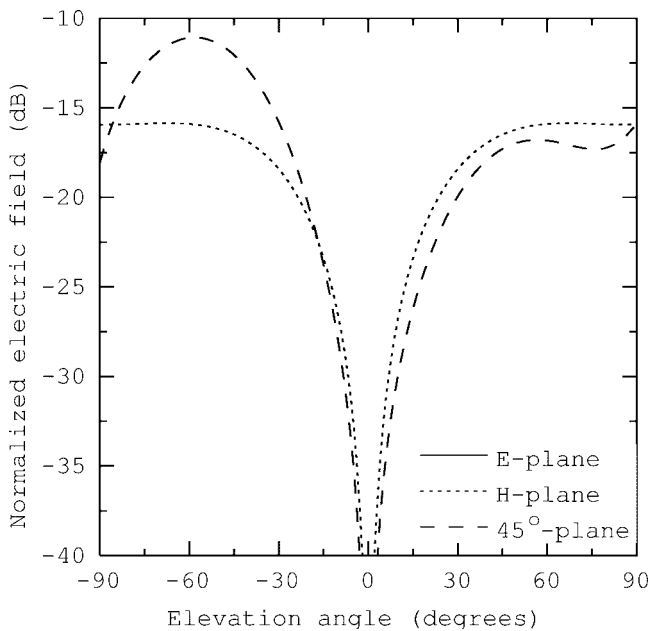Fig. 9. Model C: computed copolar patterns inside the lens at 65 GHz.

Fig. 11. Model C: computed and measured E-plane copolar patterns at 70 GHz.

Fig. 10. Model C: computed cross-polar patterns inside the lens at 65 GHz.

Fig. 12. Model C: computed and measured H-plane copolar patterns at 70 GHz.

surface is 57% and the corrected directivity is $D = 29.4$ dB. Due to this high reflection, which was not considered in the computation of η_g, the power level away from the beam is higher than computed. Consequently, D and η_g estimated from measurements conducted in planes E, H, and diagonal (45°) are, respectively, 27.7 dB and 62%. Indeed, when the power outside the main beam region is not considered, estimated D and η_g increase to the level of the theoretical predictions. For example, if only a 30° angular sector centered on the system axis is considered (which takes into account the main lobe and the first two secondary lobes on each side), the D estimate from measurements increases from 27.7 to 29.2 dB and the η_g estimate increases from 62 to 84.5%. The worst x-pol level has been measured (as expected) in the diagonal plane, the
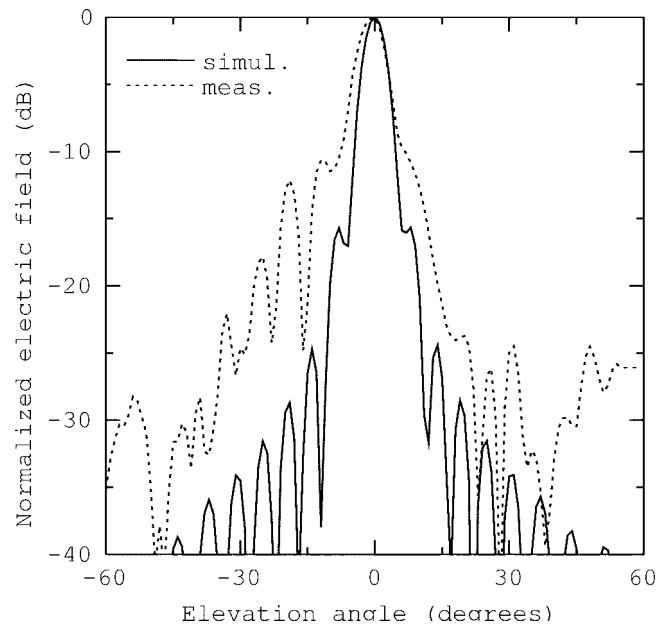
highest value being -10.9 dB. This slightly high figure is due to a combination of three factors. First, the antenna has been optimized for maximum power transfer to the mixing diode; therefore, a standing wave exists in the CPW line because the standing wave ratio (SWR) is not zero. Second, the small asymmetries due to the manufacturing process multiply the influence of the standing wave. Finally, the multiple reflections that take place inside the lens because of the low transmission efficiency also contribute significantly to the x-pol level. This problem, as well as that of reduced D and η_g, could be effectively overcome by a matching cap layer. Indeed, it has been computed that a uniform layer of thickness 0.65 mm and
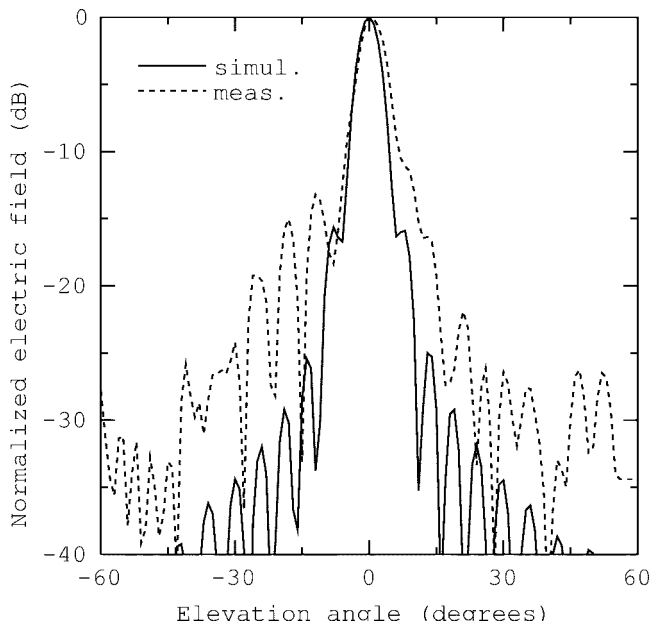
Fig. 13. Model C: computed and measured E-plane copolar patterns at 72 GHz.

relative permittivity $\epsilon_r = 3.6$ would increase the transmission efficiency of the hyperhemispherical lens from 70 to 97% and that of a synthesized ellipsoidal lens from 52 to 73%. Such efforts are underway in our laboratory based on a corrugated matching surface.

V. CONCLUSIONS

A modified rectangular loop-slot antenna with built-in tuning and dc-return capabilities, printed on the back surface of a dielectric extended hemisphere, has been presented and fully characterized. The proposed configuration is scalable up to the submillimeter-wave band because the CPW feed allows mounting the mixing diode close to the antenna. The integrated antenna exhibits tuning capabilities, a rotationally symmetric patterns, high directivity, good Gaussian coupling efficiency, and a reasonable frequency bandwidth. Three models have been simulated and one of them has been built and measured with success. Computed results show how bandwidth and pattern characteristics depend on the size parameters of the antenna. IST length, antenna feed slot width, and aspect ratio may be used to set the desired frequency and bandwidth while keeping rotationally symmetric patterns. Measured results agree with computations.

ACKNOWLEDGMENT

The authors would like to thank Prof. F. Gardiol for his detailed review of the manuscript and J.-F. Zürcher, Senior Engineer at LEMA-EPFL, who supervised the manufacturing and testing of the interested antennas.

REFERENCES

[1] D. B. Rutledge, D. P. Neikirk, and D. P. Kasilingam, "Integrated-circuit antennas," in *Infrared and Millimeter Waves*, K. J. Button, Ed. New York: Academic, 1983, vol. 10, ch. 1, pp. 1–90.

[2] S. S. Gearhart and G. M. Rebeiz, "UA monolithic 250 GHz Schottky-diode receiver," *IEEE Trans. Microwave Theory Tech.,* vol. 42, no. 12, pp. 2504–2511, Dec. 1994.

[3] C. E. Tong and R. Blundell, "An annular slot antenna on a dielectric half-space," *IEEE Trans. Antennas Propagat.,* vol. 42, pp. 967–974, July 1994.

[4] S. R. Raman and G. M. Rebeiz, "Single- and dual-polarized millimeter-wave slot-ring antennas," *IEEE Trans. Antennas Propagat.,* vol. 44, pp. 1438–1444, Nov. 1996.

[5] F. Colomb, K. Hur, W. Stacey, and M. Grigas, "Annular slot antennas on extended hemispherical dielectric lenses," in *IEEE AP-S Antennas Propagat. Int. Symp.,* Baltimore, MD, July 1996, pp. 2192–2195.

[6] J.-M. Laheurte, L. P. B. Katehi, and G. M. Rebeiz, "CPW-fed slot antennas on multilayer dielectric substrates," *IEEE Trans. Antenna Propagat.,* vol. 44, pp. 1102–1111, Aug. 1996.

[7] L. Giauffret, J.-M. Laheurte, and A. Papiernik, "Study of various shapes of the coupling slot in CPW-fed microstrip antennas," *IEEE Trans. Antennas Propagat.,* vol. 45, pp. 642–647, Apr. 1997.

[8] J. R. Mosig, "Arbitrarily shaped microstrip structures and their analysis with a mixed potential integral equation," *IEEE Trans. Microwave Theory Tech.,* vol. 36, pp. 314–323, Feb. 1988.

[9] G. V. Eleftheriades, H. LePezennec, and J. R. Mosig, "A fast and rigorous CAD procedure for complex shielded planar circuits," in *IEEE MTT-S Int. Symp. Dig.,* San Francisco, CA, June 1996, pp. 1467–1470.

[10] D. F. Filipovic, S. S. Gearhart, and G. M. Rebeiz, "Double-slot antennas on extended hemispherical and elliptical silicon dielectric lenses," *IEEE Trans. Microwave Theory Tech.,* vol. 41, pp. 1738–1749, Oct. 1993.

[11] P. Otero, G. V. Eleftheriades, and J. R. Mosig, "Loop type antennas on substrate lenses for IC millimeter-wave and submillimeter-wave mixers," LEMA-DE-EPFL, Lausanne, Final Rep., ESA/ESTEC Project 160224, Mar. 1997.

[12] N. I. Dib, "Theoretical characterization of coplanar waveguide transmission lines and discontinuities," Ph.D. dissertation, Univ. Michigan, Ann Arbor, MI, 1992.

[13] P. Otero, G. V. Eleftheriades, and J. R. Mosig. "Modeling the coplanar transmission line excitation of planar antennas in the method of moments," *Microwave Opt. Technol. Lett.,* vol. 16, no. 4, pp. 219–225, Nov. 1997.

[14] C. T. Tai, *Dyodic Green Functions in Electromagnetic Theory,* 2nd ed. New York: IEEE Press, 1994.

[15] J. R. Mosig, "Integral equation technique," in *Numerical Techniques for Microwave and Millimeter-Wave Passive Structures,* T. Itoh, Ed. New York: Wiley, 1989, ch. 3, pp. 133–213.

[16] J. R. Mosig, "Numerical analysis of microstrip patch antennas," in *Handbook of Microstrip Antennas,* J. R. James and P. S. Hall, Eds. London, U.K.: Peter Peregrinus, 1989, ch. 8, pp. 393–453.

[17] D. F. Filipovic, G. P. Gauthier, S. Raman, and G. M. Rebeiz, "Off-axis properties of silicon and quartz dielectric lens antennas," *IEEE Trans. Antennas Propagat.,* vol. 45, pp. 760–766, May 1997.

[18] P. F. Goldsmith, "Quasioptical techniques at millimeter and submillimeter wavelengths," in *Infrared and Millimeter Waves,* K. J. Button, Ed. New York: Academic, 1982, vol. 6, ch. 5, pp. 277–343.

[19] P. F. Goldsmith, "Quasi-optical techniques," *Proc. IEEE,* vol. 80, pp. 1729–1747, Nov. 1992.

[20] G. V. Eleftheriades, J. F Zürcher, and J. R. Mosig, "Patterns and efficiencies of slot-fed mm-wave glass-ceramic substrate lens antennas," in *Proc. ESA/ESTEC Workshop Millimeter-Wave Tech. Appl.,* Noordwijk, The Netherlands, Nov. 1995, pp. 22.1–22.13.

[21] S. E. Schwarz, "Efficiency of quasioptical couplers," *Int. J. Infrared Millimeter Waves,* vol. 5, no. 12, pp. 1517–1525, Dec. 1984.

[22] G. M. Rebeiz, "Millimeter-wave and terahertz integrated circuit antennas," *Proc. IEEE,* vol. 80, pp. 1748–1770, Nov. 1992.

Pablo Otero was born in Spain in 1958. He received the Ing. Telecomun. degree from the Polytechnic University of Madrid, Spain, in 1983.

After ten years in different Spanish companies, (Standard Eléctrica, E. N. Bazán, and Telefónica Sistemas), he joined the University of Seville, Spain, as a Lecturer where he taught a course on propagation of radiowaves for two years, from 1993 to 1995. In 1996, he joined the Laboratory of Electromagnetics and Acoustics of the Swiss Federal Institute of Technology at Lausanne (EPFL), Switzerland, under a grant by the Spanish Government. His primary research interest is in millimeter-wave antennas and circuits for short-range and indoor wide-band communications.

George V. Eleftheriades (S'85–M'94) was born in Limassol, Cyprus. He received the Dipl. degree in electrical engineering (with distinction) from the National Technical University of Athens, Greece, in 1988, and the M.S. and Ph.D. degrees in electrical engineering, both from the University of Michigan, Ann Arbor, in 1989 and 1993, respectively.

From 1994 to 1997, he was a Research Associate at the Laboratory of Electromagnetics and Acoustics of the Swiss Federal Institute of Technology at Lausanne (EPFL). In 1997, he joined the Department of Electrical and Computer Engineering of the University of Toronto, Canada, where he is currently an Assistant Professor. His present research interests include millimeter-wave antennas and circuits for wireless applications, planar antennas and circuits for telecommunications, numerical and analytical techniques in electromagnetics, and high-speed digital interconnects.

Dr. Eleftheriades received the Best Paper Award at the 1990 JINA International Conference on Antennas, Nice, France, an IEEE AP-S Student Paper Award in 1993, and the "Distinguished Achievement Award" from the University of Michigan in 1991.

Juan R. Mosig (S'76–M'87–SM'94) was born in Cádiz, Spain. He received the electrical engineering degree from the Polytechnic University of Madrid, Spain, in 1973, and the Ph.D. degree from the Swiss Federal Institute of Technology at Lausanne (EPFL), Switzerland, in 1983.

In 1976, he joined the Laboratory of Electromagnetics and Acoustics of the Swiss Federal Institute of Technology at Lausanne (EPFL), Switzerland. In 1984, he was a Visiting Research Associate at Rochester Institute of Technology, Rochester, NY. He has also held scientific appointments at the Universities of Rennes, France, Nice France, Technical University of Denmark, Lyngby, and the University of Colorado at Boulder. Since 1991 he has been a Professor at EPFL. He is the author of four chapters in books on microstrip antennas and circuits. He is co-organizer and Lecturer of yearly short intensive courses in numerical electromagnetics in Europe and the United States. His research interests include electromagnetic theory, numerical methods, and microstrip antennas.

Dr. Mosig is a member of the Swiss Federal Commission for Space Applications and responsible of several research projects for the European Space Agency.